Ultrasonic Measurement of Strain Generated by Dual Acoustic Radiation Force for Evaluation of Acupuncture Therapy

Yoshitaka Odagiri, Hideyuki Hasegawa, Hiroshi Kanai
Graduate School of Engineering, Tohoku University,
Sendai 980-8579, Japan
E-mail: odagiri@us.ecei.tohoku.ac.jp

Abstract— **Many studies have been carried out on the measurement of mechanical properties of tissues by applying an ultrasound-induced acousticradiation force. To assessmechanical properties, strain of an objectmust be generated. However, use of only one radiation force is notsufficient because it also causes translational motion when the object is much harder than surrounding medium. In this study, two cyclicultrasound radiation forces are applied to a phantom which mimics muscle from two opposite horizontal directions so that the object is cyclically compressed in the horizontal direction. As a result, the object is vertically expanded due to the incompressibility. The resultant vertical displacement is measured using ultrasound and laser vibrometer. Two concave ultrasonic transducers for actuation were both driven by sums of two continuous sinusoidal signals at two slightly different frequencies of 1 MHz and (1M+5) Hz. Displacement at the surface, which fluctuates at 5 Hz, was measured by the ultrasonic *phased tracking method* proposed by our group. The displacement was also measured with laser to validate ultrasonic measurement. Results indicated that the phantom was cyclically actuated with an amplitude of tenth of a few micrometers which well coincided with that measured with laser.**

I. Introduction

Acupuncture is a kind of therapy by the insertion of very thin needles, from the skin surface in order to improve physiological functioning of the body. Figure 1 shows meridians in shoulders to alleviate the stiffness and appearanceof acupuncture therapy. Acupuncture are over 2,000 years old and has developed based on the authority of experience. However, from the view point of the Western medicine, meridians, which the acupuncture depends on, do not corresponds to nervus or blood circulation. Therefore, the acupuncture is an scientific controversial issue in the Western medicine. For this reason, quantitative evaluation of acupuncture therapy is important. Recently, some remote actuation methods based on acoustic radiation forces have been reported. Fatemi and Greenleaf proposed an imaging modality that uses the acoustic response of the object to a localized dynamic radiation force[1], [2]. The radiation force produces acoustic emission which is closely related to the mechanical frequency response of the medium. By measuring the acoustic emission with a hydrophone, hard inclusions in soft material may be experimentally detected. The spatial resolution in the depth direction corresponds to the size of the intersectional area.

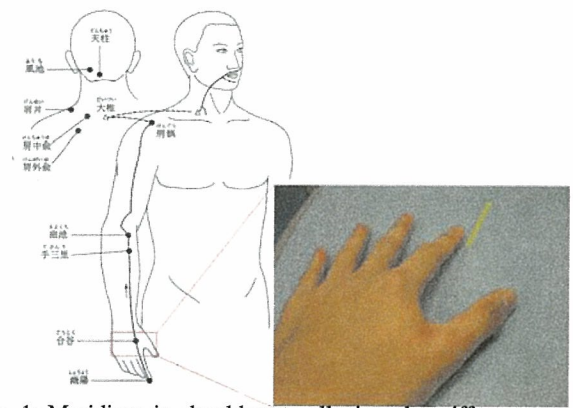

Fig. 1: Meridians in shoulders to alleviate the stiffness.

However, as shown in Fig. 2(a), one acoustic radiation force does not generate strain in an object effectively because it also causes a change in the object's position, which has zero spatial gradient in displacement. Especially when the elastic modulus of the object is far greater than that of the surrounding media, one acoustic radiation force may generate only a change in the position of the object[3]. In this study, as illustrated in Fig. 2(b), the strain on the face of an object is generated by placing it on a hard base. In addition, as illustrated in Fig. 2(c), for effective generation of strain in the object, two acoustic radiation forces respectively induced by two ultrasounds at frequencies f and $f + \Delta f$ were applied to two different positions in the object from two different directions. In this study, the displacement generated by acoustic radiation forces was measured by the ultrasonic *phased tracking method*[4] and a laser Doppler velocimetory.

II. Principle

As illustrated in Fig. 3, when the ultrasound propagates in a medium, a constant force is generated in the direction of propagation. This force is called as the acoustic radiation force[5]. The acoustic radiation pressure, $P_R(t)$, is defined as the acoustic radiation force per unit area as follows:

$$p_R(t) = (1 + R^2)e(t), \tag{1}$$

where R and $e(t)$ are the pressure reflection coefficient and the energy density at the interface, respectively. In eq. (1), the

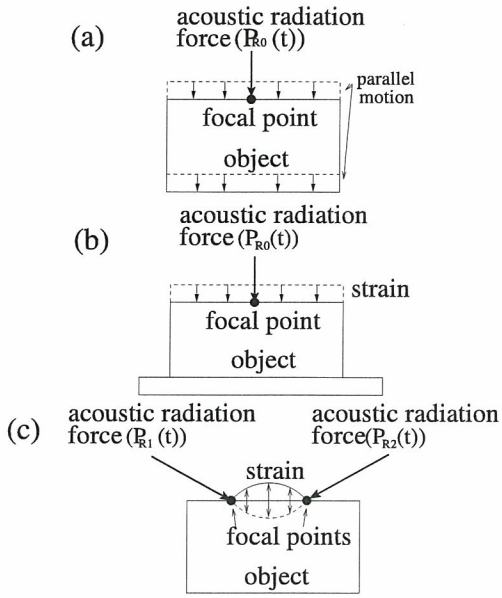

Fig. 2: Illustrations of (a) the change in position of an object caused by only one acoustic radiation force, (b) the strain of an object fixed on a hard base caused by an acoustic radiation force, and (c) the strain of an object caused by two acoustic radiation forces.

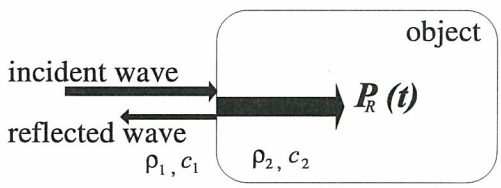

Fig. 3: A model of the acoustic radiation force exerted on the interface of the object

transmitted wave is assumed to be perfectly absorbed in the object. Using the densities, ρ_1 and ρ_2, and sound speeds, c_1 and c_2, of the medium and the pbject, the reflection coefficient, R, and the energy density, $e(t)$, are defined by

$$R = \frac{z_2 - Z_1}{z_2 + Z_1} = \frac{\rho_2 c_2 - \rho_1 c_1}{\rho_2 c_2 + \rho_1 c_1} \tag{2}$$

$$e(t) = \frac{1}{\rho_1 c_1^2}\{p(t)\}^2 \tag{3}$$

The energy density, $e(t)$, of the incident wave is proportional to the square of the sound pressure, $p(t)$, of the ultrasound beam. When two ultrasounds with the same sound pressure, p_0, at slightly different frequencies, f and $f + \Delta f$, are crossed each other, an acoustic radiation pressure which fluctuates at the frequency difference, Δf, is generated in the intersectional area. In this case, the sound pressure, $p_{sum}(t)$, in the intersectional area is expressed as follows:

$$p_{sum}(t) = p_0 \cos 2\pi f t + p_0 \cos 2\pi (f + \Delta f)t, \tag{4}$$

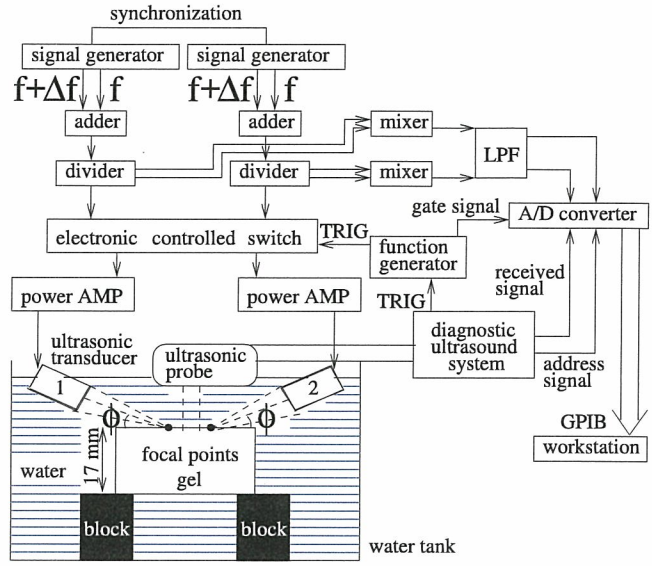

Fig. 4: Measurement system.

For this case, the energy density, $e(t)$, is expressed as follows:

$$\begin{aligned} e(t) &= \frac{1}{\rho_1 c_1^2}\{p_{sum}(t)\}^2 \\ &= \frac{1}{\rho_1 c_1^2}\{p_0 \cos 2\pi f t + p_0 \cos 2\pi (f + \Delta f)t\}^2 \\ &= \frac{p_0^2}{\rho_1 c_1^2}\{1 + \cos 2\pi \Delta f t + \cos 2\pi (2f + \Delta f)t \\ &\quad + \frac{1}{2}\cos 4\pi f t + \frac{1}{2}\cos 4\pi (f + \Delta f)t\}, \end{aligned} \tag{5}$$

From the second term of the right-hand side of eq. (5), it is found that the energy density, $e(t)$, has a component at the frequency difference Δf. With respect to the low-frequency component, the acoustic radiation pressure, $P_R(t)$, acting on the interface is given by

$$P_R(t) = (1 + R^2)\frac{p_0^2}{\rho_1 c_1^2}(1 + \cos 2\pi \Delta f t), \tag{6}$$

where R is the pressure reflection coefficient on the surface of the object.

To improve the spatial resolution in measurements of the response of an object, an ultrasound correlation-based method, the ultrasonic *phased tracking method*, is used to measure the minute displacement, $d(t)$, caused by the acoustic radiation force[6]. The accuracy in the displacement measurement by the *phased tracking method* was evaluated to be 0.2μm by basic experiments using a rubber plate[7], and influences of the focal position of the ultrasonic beam and the change in center frequency of RF echo due to the frequency-dependent attenuation in tissue on the measurement accuracy were also investigated.

III. Experimental Setup

The measurement system is illustrated in Fig. 4. In order to measure the strain, we employed ultrasonic diagnostic equip-

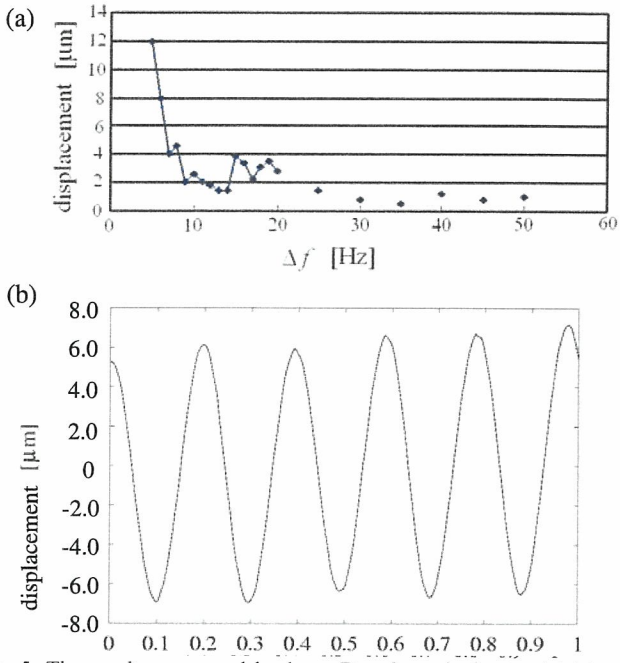

Fig. 5: The results measured by laser Doppler velocimetry (a) Maximal displacement generated by difference of Δf. (b) Displacement measured at frequency difference, 5 Hz.

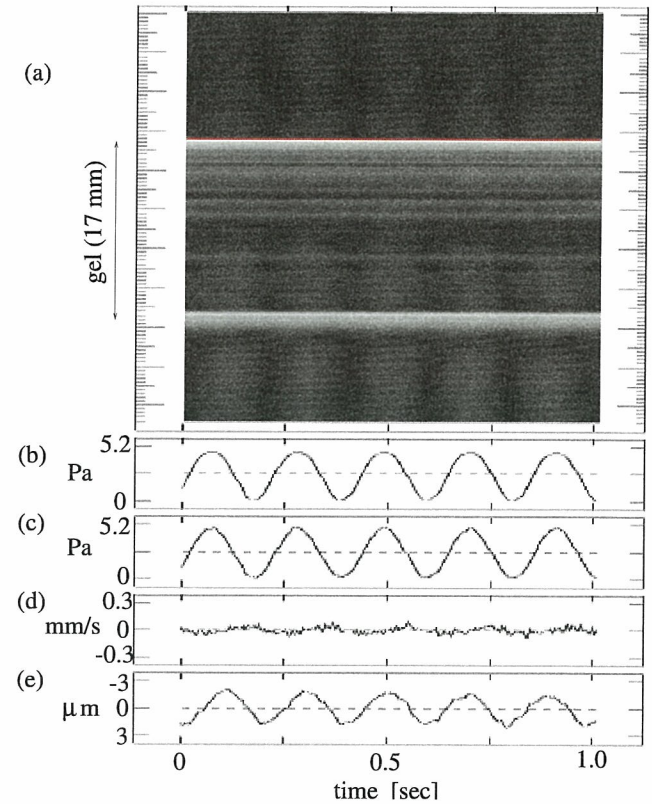

Fig. 6: (a) M-mode image of an object. (b) Acoustic radiation pressure, $P_{R1}(t)$. (c) Acoustic radiation pressure, $P_{R2}(t)$. (d) The Vibration velocity of the object. (e) Displacemant of the object.

ment (Toshiba SSH-160A) with a linear-type probe (center frequency: 3.75 MHz). The equipment was modified to detect the minute displacement of the object by the ultrasonic *phased tracking method.* Two concave ultrasonic transducers were driven by a sum of two continuous waves (CWs) at two slightly different frequencies of 1 MHz and 1 MHz+Δf Hz. The resultant ultrasound beams were focused at 50 mm away from the surface of the transducer with a beam angle ϕ. The displacements of the object, where the two acoustic radiation forces were applied, were measured by the ultrasonic *phased tracking method* [3]. The gel, which is phantom of muscle, for the practice of acupuncture was used as the object.

When CW ultrasound is employed for actuation, interference occurs between the CW ultrasound for actuation and the pulsed ultrasound for displacement measurement. In order to avoid this interference, an electrical switch to control the cessation of the CW ultrasound for actuation is used.

In this study, the amplitude of displacement was measured at each frequency difference, Δf. Then, the displacement of the object, in the case that one acoustic radiation force was applied, was measured by a laser Doppler velocimetry to check the actuation. When a laser Doppler velocimetry was used, reflection theet was pasted on the face of object to measure surface velocity. In this case, focal point of an acoustic radiation force was set at boundary with the reflection theet because the pressure reflection coefficient, R, changes when an acoustic radiation force is exerted on the face of reflection theet.Finally, regional strain was generated in the object efficiently using two focused ultrasonic transducers.

IV. Results

The maximal amplitude of displacement generated an acoustic radiation force at Δf is shown in Fig. 5(a). When Δf is 5 Hz, the amplitude was maximum, and rapidly decreases at higher frequencies. This is explained by the fact that the dynamic loss elastic modulus increases depending on frequency. In the frequency range from 1 Hz to 4 Hz, the displacement could not be measured because of the property of the laser Doppler. Figure 5(b) shows displacement measured at frequency difference, 5 Hz.

The displacement generated by using dual acoustic radiation forces was measured with ultrasound. In this experiment, the difference frequency, Δf, employed 5 Hz and angles, ϕ set to 25 degrees. Focal points of two transducers set at same position. Figures 6(a) shows the M-mode images of the object. Acoustic radiation pressures, $P_{R1}(t)$ and $P_{R2}(t)$, shown in Figs. 6(b) and 6(c) were moved in the same phase. Figure 6(d) shows the vibration velocity of the object obtained by the *phased tracking method.* By integrating the velocities, the displacement was obtained as shown in Fig. 6(e). The amplitude of the measured displacement was about 4.0 μm. From these results, using the proposed method, the regional strain was successfully generated and measured with ultrasound.

Displacement at each beam position is shown in Fig. 7. In this study, linear-type probe (center frequency: 3.75 MHz) was employed when displacement was measured by ultrasound.

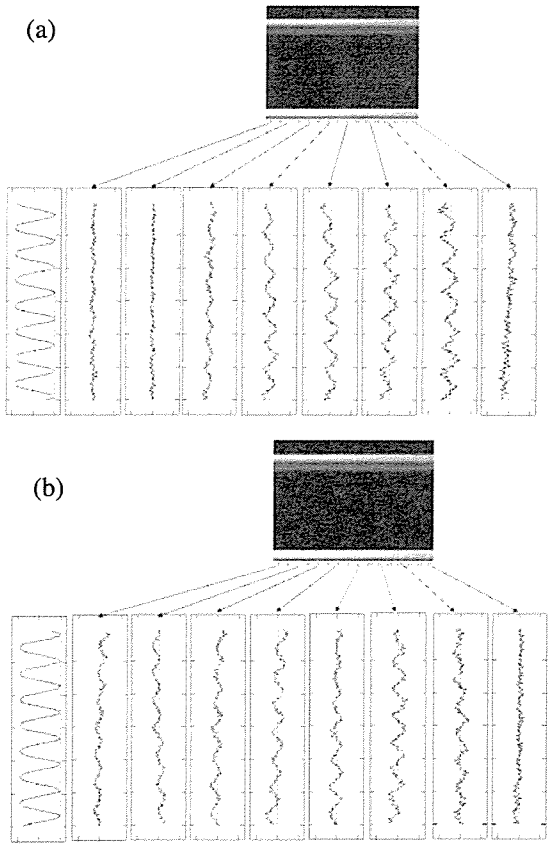

Fig. 7: Displacement at each beam position (a) focal points set at same position. (b) distance of focal point set to 10 mm.

Therefore, 16 positions can measure at one ultrasonic measurement. Displacement, when two focal points set at the same position, is shown in Fig. 7(a). Amplitude of displacement is higher in the vicinity of overlapping focal point than other position. Displacement, when distance of focal point set to 10 mm, is shown in Fig. 7(b). Displacement are more widely distributed than that Fig. 7(a). this shows that force such as pinch was applied.

V. Conclusion

In this paper, the displacement generated by acoustic radiation force was measured by ultrasonic probe and the laser Doppler velocimetry, and these results was same order, μm. It was shown that strain could be measured by using the ultrasonic *phased tracking method*.In addition, it was shown that regional strain was generated on the object using two focused ultrasonic transducers. These results show a potential of the proposed method for generation of the regional strain on the muscle.

References

[1] M.Fatemi, and J.F.Greenleaf, "Vibro-Acoustic Mammography," *IEEE Transactions on Medical Imaging*, Vol. 21, pp. 1-8, 2002.

[2] M.Fatemi, and J.F.Greenleaf, "Vibro-acoustgraphy: An imaging modality based on ultrasound-stimulated acoustic emission," Proceedings of the National Academy of Sciences of the United States of America, Vol.96, pp. 6603-6608, 1999.

[3] H. Hasegawa, M. Takahashi, Y. Nishio and H. Kanai, "Generation of Strain Inside Object Using Dual Acoustic Radiation Force," *Japanese Journal of Applied Physics*, Vol. 45, pp.4706-4711, 2006.

[4] H.Kanai, M. Sato, Y. Koiwa, and N. Chubachi, "Transcutaneous Measurement and Spectrum Analysis of Heart Wall Vibrations," *IEEE Transactions on Ultrasonics, Fellowelectrics, and Frequency Control*, Vol. 43, pp. 791-810, 1996.

[5] G. R. Torr, "The acoustic radiation force," *American Journal of Physics*, Vol. 52, pp. 402-408, 1984.

[6] K. Michishita, H. Hasegawa and H. Kanai, "Ultrasonic Measurement of Minute Displacement of Object Cyclically Actuated by Acoustic Radiation Force," *Japanese Journal of Applied Physcis*, Vol. 42, pp. 4608-4612, 2003.

[7] H. Kanai, K. Sugimura, Y. Koiwa, and Y. Tsukahara, "Accuracy Evaluation in Ultrasonic-based Measurement of Microscopic Change in Thickness" *Electronics Letters*, Vol. 35, pp. 949-950, 1999.

Measurement of Angle-Dependent Ultrasound Scattering from Wire Phantom Mimicking Myocardial Fiber

Teppei Onodera, Hideyuki Hasegawa, Hiroshi Kanai
Graduate School of Engineering, Tohoku University,
Sendai 980-8579, Japan
E-mail: onodera@us.ecei.tohoku.ac.jp

Abstract— **A difference between a normal and hypertrophic hearts is whether the direction of regional myocardial fibers are homogeneously aligned along one direction or not. In order to investigate the angle dependence of ultrasonic scattering in relation to the fiber direction, we measured the ultrasonic echoes from a metal wire phantom, which mimics a bundle of myocardium fibers, as a function of the insonification angle. In this study, we focused on ultrasonic scattering properties in relation to the azimuth and elevation angles of insonification and receiving. Experimental results showed that the amplitude of the reflected echo from the metal wire became the maximum when the ultrasonic beam was insonified parallel to the direction of fibers. In the case of the parallel insonification, echoes from the wire showed directivity like those from an interface. Such a directivity was considered to contribute to the dependence of echoes on the azimuth angle.**

I. Introduction

Directions of myocardial fibers in a normal human heart wall change gradually from the epicardium to the endocardium and are homogeneously aligned in each plane which is parallel to the luminal surface of the heart wall. [1] However, in a heart wall affected by the hypertrophic heart disease, the myocardial fiber direction becomes disarrayed. [2] Therefore, it is important to diagnose the myocardial fiber direction for differentiation of normal hearts from those affected by the hypertrophic heart disease. It is expected that ultrasonic scattering from a heart wall characterizes such a change in the direction of myocardial fiber. Basic researches based on backscattered echoes from myocardium have been conducted for the quantitative tissue characterization. [3]

In order to quantify the correspondence between the acoustic properties of an object and ultrasonic backscattering, Knipp *et al.* made use of a reference phantom of known acoustic properties for measuring ultrasonic backscattering with eliminating influences of the measurement system. [4], [5] Baldwin *et al.* measured the ultrasonic myocardial attenuation with changing the angle of ultrasonic propagation relative to the myocardial fibers for the quantitative ultrasonic cardiac tissue characterization. [1], [3] By measuring ultrasonic backscattering from myocardium at each insonification angle θ relative to the direction of the myocardial fibers, it is shown that the ultrasonic attenuation in the myocardium is maximum when θ is zero (parallel) to the myocardial fibers and it has the minimum when θ is 90° (perpendicular) to the fibers. In previous studies, it was found that ultrasound integrated backscatter from myocardium exhibits cyclic variation during one cardiac cycle. [6], [7], [8], [9] One of the reasons is considered to be the change of the angle between the ultrasonic beam and the direction of myocardial fibers. [10]

In this study, we focused on ultrasonic scattering properties in relation to the azimuth and elevation angles of insonification relative to the fiber direction. For this purpose, ultrasonic echoes from a wire phantom (with a diameter of less than the wavelength) which mimics a bundle of myocardium fibers were measured as a function of the insonification angle.

II. Methods

An experimental setup is illustrated in Fig. 1. As shown in Fig. 1(a), two focused transducers were used for transmitting and receiving. The transmitting and receiving elevation angles are ϕ_1 and ϕ_2, respectively. In this paper, ultrasonic echoes from a wire phantom were measured with changing the angles, ϕ_1, ϕ_2, and azimuth angle θ. During the experiment, focal points of these transducers are required to be set at the same point on the phantom. By keeping the focal points at the same point, the object was revolved around that point to change the azimuth angle θ. Furthermore, the elevation angle ϕ was changed by moving the transducers along a circle whose center is the same point on the phantom. To realize such operations, a custom-made apparatus was used. The measurement apparatus is shown in Fig. 1(b).

Both transducers for transmission and reception are single element concave transducers (Tokimec 7Z10I-PF30-C-K445). Focal distances of the transducers were 30 mm and the center frequency is 7.0 MHz. The wire phantom was placed in a water tank as shown in Fig. 1(b) and was fixed on the center of the cylindrical pedestal. The azimuth angle of insonification relative to the fiber direction was changed by rotating the pedestal. There was a hole of 20 mm in diameter at the center of the top of the pedestal in order to receive only the signal reflected from the object. Burst sine waves of

one cycle were applied to the transmitting transducer. The signals reflected from the object were received by the receiving transducer. The digitized data were acquired after averaging the reflected signals 128 times using a digital oscilloscope (Tektronix TDS220).

III. Results

The diameter of a human myocardial fiber (10-15 μm)[5] is thinner than the wavelength of ultrasound (400-500 μm) used in ultrasonic diagnostic equipment. Therefore, ultrasonic echoes from human myocardium fibers are scattered waves. The object use in this study was a copper wire of about 170 μm in diameter. The wavelength of insonified ultrasound was 214 μm. Thus, ultrasonic echoes were also scattered waves.

Figure 2 shows the received RF signals, when the ultrasonic beam was insonified parallel to the wire ($\theta = 0°$), at two settings of the elevation angles ($\phi_1 = \phi_2 = 30°$ and $50°$). As shown in Fig. 3, the peak value was measured at each setting of the azimuth and elevation angles.

Figure 3 shows the angular dependence of the maximum amplitude of the reflected signals at each azimuth angle, θ. The amplitude of the reflected signal changed with azimuth angle, θ. Although the pedestal was revolved three times, reproducible measurement were done with respect to the azimuth angle, θ. At the same elevation angle ($\phi_1 = \phi_2$), the amplitude became the maximum when the ultrasonic beam was insonified parallel to the wire ($\theta = 0°$ and $180°$). On the other hand, when the ultrasonic beam was insonified perpendicularly to the wire ($\theta = 90°$ and $180°$), the amplitude tended to be the smallest.

Figure 4 shows the change of the maximum amplitude of the received signals at each deference in elevation angles ($\phi_2 - \phi_1$). The azimuth angle θ was kept at $90°$ in Fig. 4(a) and $\theta = 0°$ in Fig. 4(b), respectively. Amplitude profiles, amplitudes showed the similar tendency at each insonification elevation angle ϕ_1.

In the case of insonification perpendicular to the wire ($\theta = 90°$), the amplitude does not change so much with respect to $\phi_2 - \phi_1$, and decreases as the angle diffrenece ($\phi_2 - \phi_1$) increases. On the other hand, in the case of insonification pararell to the wire direction ($\theta = 0°$), amplitudes became the maximum when the angle difference ($\phi_2 - \phi_1$) is zero degree. When the absolute value of the angle difference is more than 20 degrees, the amplitudes was almost zero.

Figure 5 shows the echo amplitude from an flat aluminum plate measured by similar procedure as in Fig. 4(b). Echoes from an aluminum plate were the maximum when the angle difference ($\phi_2 - \phi_1$) is zero. When the absolute value of the angle difference is more than 20 degrees, the amplitudes were also almost zero. These results suggest that the wire acts as an interface in the case of parallel insonification ($\theta = 0°$).

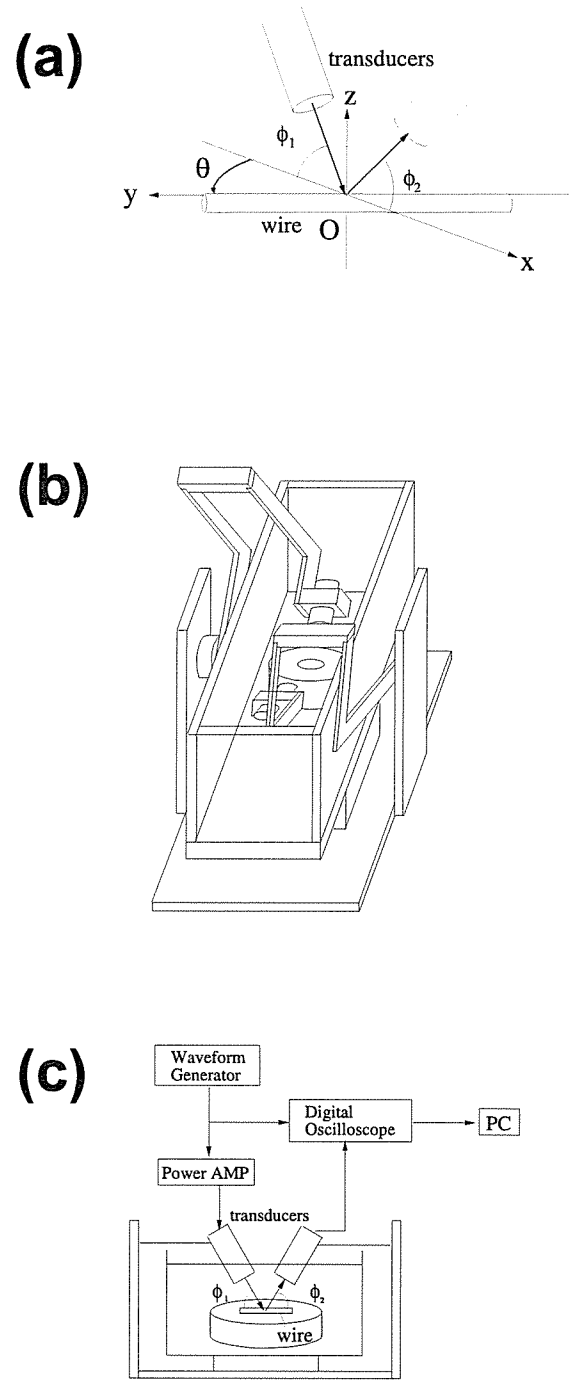

Fig 1: Illustrations of (a) the measurement, (b) a custom-made apparatus, and (c) experimental setup.

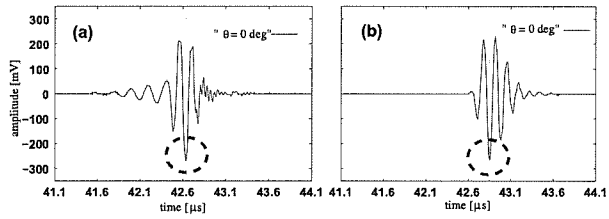

Fig. 2: Examples of the received signals from the wire ($\theta = 0°$). (a) $\phi_1 = \phi_2 = 30°$. (b) $\phi_1 = \phi_2 = 50°$. vspace5mm

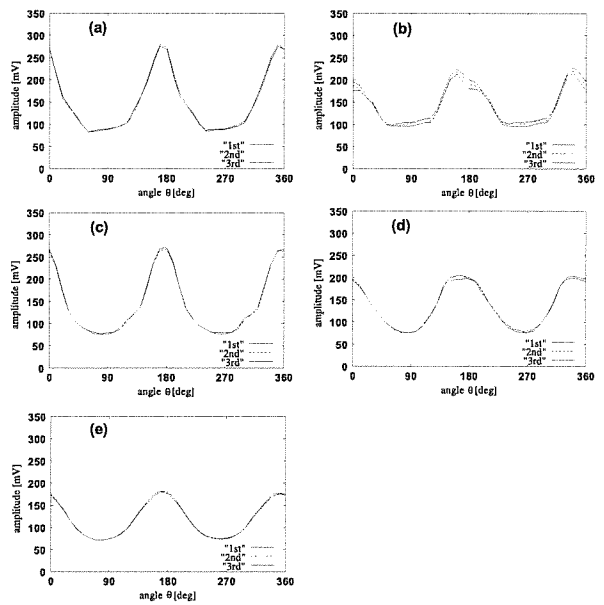

Fig. 3: Maximum amplitude of the received signals at each azimuth angle θ. (a) $\phi_1 = \phi_2 = 30°$. (b) $\phi_1 = \phi_2 = 40°$. (c) $\phi_1 = \phi_2 = 50°$. (d) $\phi_1 = \phi_2 = 60°$. (e) $\phi_1 = \phi_2 = 70°$.

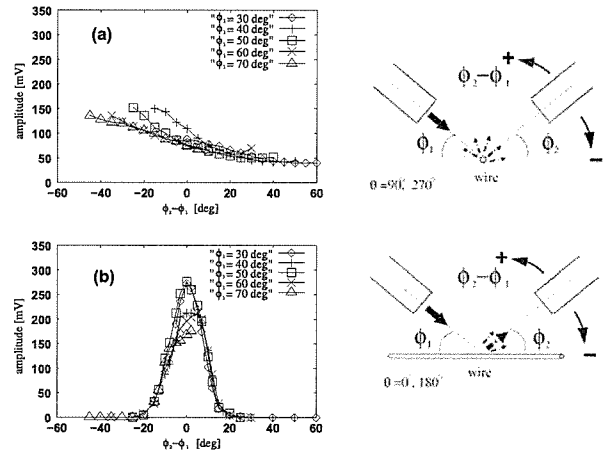

Fig. 4: Maximum amplitude of the received signals at each angle difference $\phi_2 = \phi_1$ between receiving and insonification elevation angles, ϕ_1 and ϕ_2. (a) $\theta = 0°$. (b) $\theta = 90°$.

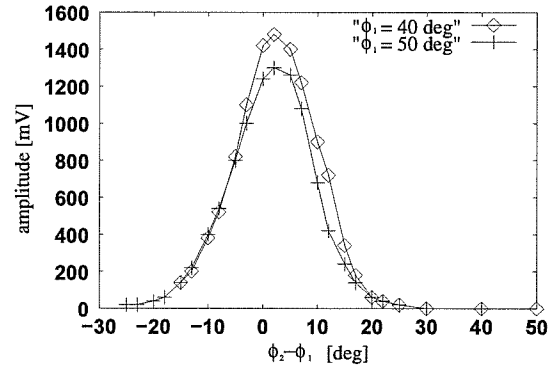

Fig. 5: Maximum amplitude of the received signals from an alminum plate at each angle difference ($\phi_2 - \phi_1$).

IV. Conclusion

In this study, in order to investigate the angle dependence of ultrasonic scattering from the wire, we constructed an experimental system to change the elevation and azimuth angles. The amplitude of the reflected signal from the wire changed with azimuth angle, θ.

The maximum amplitude of the received signals at each angle deference ($\phi_2 - \phi_1$), was not changed so much by the insonification elevation angle ϕ_1, in the case of insonification perpendicular to the wire ($\theta = 90°$). On the other hand, in the case of insonification parallel to the wire ($\theta = 0°$), the wire acts as an interface. Such a difference in amplitude profiles with respect to the angle difference between transmitting and receiving elevation angles suggests the cause of the dependence of echo on the azimuth angle.

References

[1] D. E. Sosnovik, S. L. Baldwin, S. H. Levis, M. R. Holland and J. G.Miller: Ultrasound Med. Biol. **27** (2001) 1643.
[2] J. G. Murphy: " Mayo Clinic Cardiology Review" , A Wolters Kluwer Company (2000) 455.
[3] S. L. Baldwin, K. R. Marutyan, M. Yang, K. D. Wallace, M. R. Holland and J. G. Miller: Ultrasound Med. Biol. **31** (2005) 477.
[4] T. J. Hall, J. A. Zagzebski and E. L. Madsen: Ultrason. Imag. **7** (1985) 103.
[5] J. A. Knipp, T. A. Wilson, F. Dong and E. L. Madsen: Ultrason. Imag. **19** (1997) 221.
[6] H. Kanai, Y. Koiwa, S. Katsumata, N. Izumi and M. Tanaka: Jpn. J. Appl. Phys. **42** (2003) 3239.
[7] B. Barzilai, E. I. Madaras, B. E. Sobel, J. G. Miller and J. E. Perez: Am. J. Physiol. **247** (1984) H478.
[8] E. I. Madaras, B. Barzilai, J. E. Perez, B. E. Sobel and J. G. Miller: Ultrason. Imag. **5** (1983) 229.
[9] R. M. Glueck, J. G. Mottley, J. G. Miller, B. E. Sobel and J. E. Perez: Circulation **68** (1983) III-330.
[10] S. A. Wickline, E. D. Verdonk, A. K. Wong, R. K. Shepard and J. G. Miller: Circulation **85** (1992) 259.
[11] V. J. Ferrans, A. G. Morrow and W. C. Roberts: Circulation **45** (1972) 769.
[12] F. Rushmer: "Cardiovascular Dynamics," WB Saunders (1976) 78.

Classification of Flow-limiting Thrombus in Acute Coronary Syndromes by High-frequency Acoustic Microscopy

Hidehiko Sasaki, Takayuki Kanno
Miyagi Cardiovascular and Respiratory Center
Kurihara, Japan

Yoshifumi Saijo, Motonao Tanaka
Institute of Development, Aging and Cancer, Tohoku University
Sendai, Japan

***Abstract*— Background: Virtual Histology- intravascular ultrasound (VH-IVUS) has the ability to help us distinguish between stable and unstable coronary plaques, but provides a limited definition of vulnerability on a size scale less than 100 m. The purpose of this study is to identify the acoustic properties of flow-limiting thrombus responsible for acute coronary syndromes(ACS) at the microscopic level. Methods: Acoustic microscopy operating in the high frequency range was used to display the two-dimensional distributions of color-coded images of attenuation and sound speed. A total of 26 cases of ACS patients were investigated. The tissues were sectioned at 5 mm thickness and mounted onto glass slides, were neither covered by slips nor stained. Results: The values of attenuation constant and sound speed for the red-thrombus were significantly higher than those for the platelets-rich thrombus. Both acoustic parameters for old red-thrombus were significantly lower than those for the organized thrombus. Conclusions: The acoustic properties of the flow-limiting thrombus at different stages of pathology can be classified by high-frequency acoustic microscopy. These criteria will hopefully provide a information regarding the development of a new IVUS.**

Keywords-acute coronary syndrome; thrombus; acoustic microscopy; attenuation; sound speed

I. INTRODUCTION

Virtual Histology- intravascular ultrasound (VH-IVUS) can distinguish stable and unstable coronary plaques, but it provides limited information on thrombus in coronary atherosclerosis. The purpose of this study is to clarify the acoustic properties of coronary thrombi at the microscopic level.

II. METHOD

A. Sound Speed Acoustic Microscopy

A SAM system specially developed in Tohoku University, operating in the frequency range of 50-150 MHz, was used for this study [1-6]. The sections for SAM measurements were mounted on glass slides but not covered by cover slips. The paraffin was removed from the sections by the graded alcohol method prior to the ultrasonic measurement. Distilled water was used as the coupling medium, which maintained the specimen at 20˚C during the measurement procedure. A single ultrasound pulse of 5 ns width was emitted and received by the same transducer above the specimen. The reflection from the tissue surface and that from the interface between the tissue and glass were introduced into a personal computer using a high-speed A/D converter (DP210, Acqiris, Switzerland). The sampling speed was 2 GSa/s and the resolution was 8-bit. Eight values of the time taken for a pulse response at the same point were averaged in order to reduce the noise in the measurement. The transducer was mounted on an X-Y stage with a microcomputer board that was controlled by the personal computer. Both X-scan and Y-scan were driven by linear servo motors. The area of measurement was 2.4x2.4 mm with 300x300 pixels.

Figure 1 is the block diagram of the sound speed microscopy.

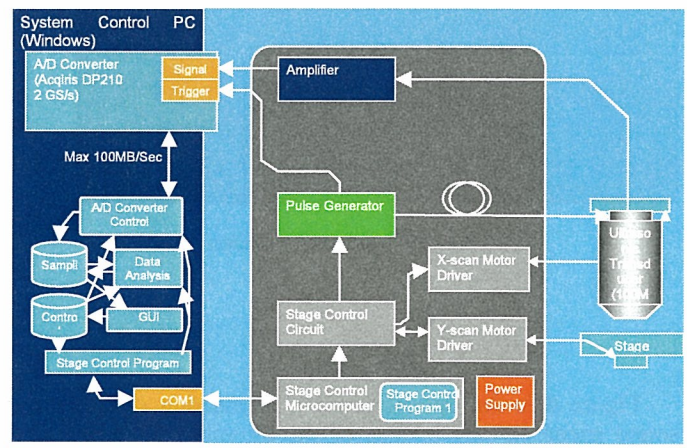

Figure 1. Block diagram of the sound speed microscopy

B. *Sample for Measurement*

Thirty-nine patients with coronary artery disease who received percutaneous coronary intervention were investigated. Tissues were retrieved from the coronary artery by aspiration catheter system (Thrombuster®) or directional coronary atherectomy procedures. The tissues for acoustic microscopy were fixed by 10% formalin, sectioned at 4 μm thickness and mounted onto glass slides without cover slips or staining. A neighboring section of the specimen was stained with Elastica-masson staining and observed by light microscopy. Figure 2 shows the appearance of the thrombus aspiration catheter system. Figure 3 shows the aspirated thrombus by the system.

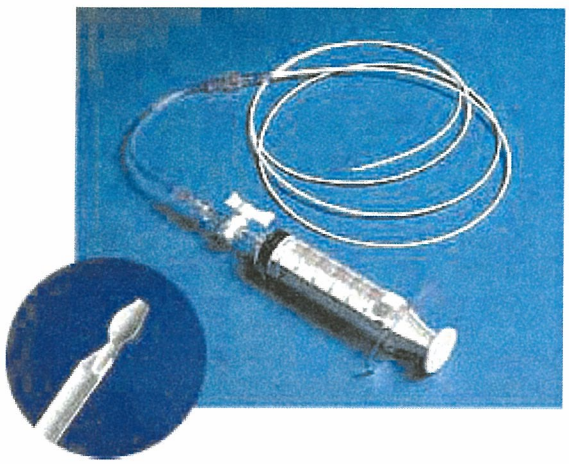

Figure 2. Apperance of thrombus aspiration cathter

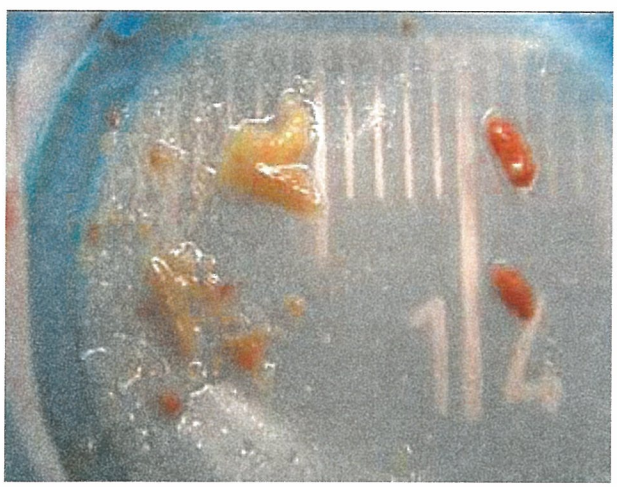

Figure 3. Aspirated thrombus

III. RESULTS

Figure 4 is the optical (upper), attenuation (middle) and sound speed (lower) images of the thrombus 50 hours after AMI onset.

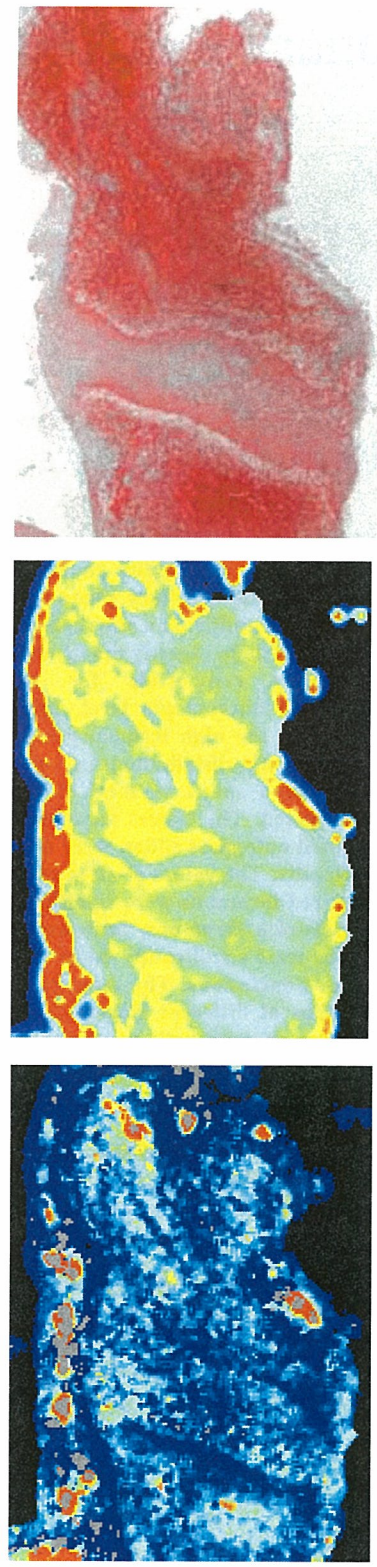

Figure 4. Optical (upper), attenuation (middle) and sound speed (lower) images of the thrombus 50 hours after AMI onset.

Figure 5 is the optical (upper), attenuation (middle) and sound speed (lower) images of the thrombus 19 hours after AMI onset.

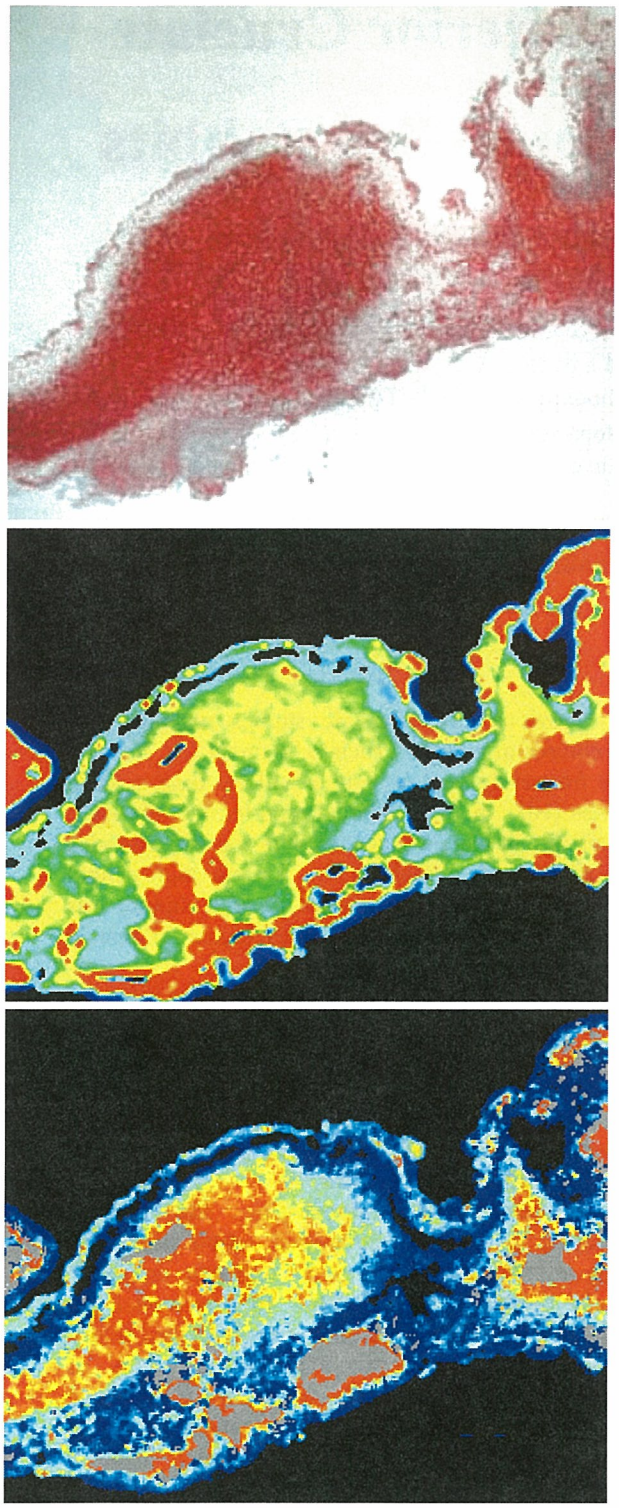

Figure 5. Optical (upper), attenuation (middle) and sound speed (lower) images of the thrombus 19 hours after AMI onset.

The values of attenuation constant and sound speed of the fresh red-thrombus were significantly higher than those of the fresh white-thrombus. Both parameters of red-thrombus decreased gradually after thrombus formation, and both parameters increased again with the organization with collagen fibers. Both parameters were high in the lesion of infiltration of inflammatory cells.

IV. Conclusion

The acoustic properties of thrombus at different stages of pathology can be classified by scanning acoustic microscopy. These criteria will provide a basis for the interpretation of conventional and VH-IVUS.

Acknowledgment

This study was supported by Grants-in-Aid for Scientific Research (Scientific Research (B) 13557059, 15300178) from the Japan Society for the Promotion of Science, Health and Labor Sciences Research Grants from the Ministry of Health, Labor and Welfare for the Research on Advanced Medical Technology (H17-Nano-001) and The Grant on Three Dimensional Organ Regeneration Program from New Energy and Industrial Technology Development Organization.

References

[1] Saijo Y, Jorgensen CS, Falk E. Ultrasonic tissue characterization of collagen in lipid-rich plaques in apoE-deficient mice. Atherosclerosis Vol. 158, No. 2; 289-295, 2001.

[2] Saijo Y, Ohashi T, Sasaki H, Sato M, Jorgensen CS, Nitta S. Application of scanning acoustic microscopy for assessing stress distribution in atherosclerotic plaque. Ann Biomed Eng, Vol. 29, No. 12, 1048-53, 2001.

[3] Sasaki H, Saijo Y, Tanaka M, Nitta S. Influence of tissue preparation on the acoustic properties of tissue sections at high frequencies. Ultrasound Med Biol, Vol. 29, No. 9, 1367-72, 2003.

[4] Hozumi N, Yamashita R, Lee CK, Nagao M, Kobayashi K, Saijo Y, Tanaka M, Tanaka N, Ohtsuki S. Time–frequency analysis for pulse driven ultrasonic microscopy for biological tissue characterization. Ultrasonics, Vol. 42, No. 1-9, 717-722, 2004.

[5] Saijo Y, Sasaki H, Hozumi N, Kobayashi K, Tanaka M, Yambe T. Sound speed scanning acoustic microscopy for biomedical applications. Technol Health Care. Vol. 13, No. 4: 261-7, 2005.

[6] Saijo Y, Hozumi N, Lee C, Nagao M, Kobayashi K, Oakada N, Tanaka N, Santos Filho ED, Sasaki H, Tanaka M, Yambe T. Ultrasonic speed microscopy for imaging of coronary artery. Ultrasonics. 2006 Jul 3; [Epub ahead of print]

Tissue Sound Speed of Anterior Cruciate Ligament in Estrogen-Controlled Rabbits

- A Measurement using the Scanning Acoustic Microscope -

Hirotaka Sano, MD[1)], Koshi Hattori, MD[1)], Tatsuro Komatsuda, MD[2)], Yoshifumi Saijo, MD[4)], Takehiko Sugita[3)], MD and Eiji Itoi, MD[1)]
Departments of Orthopaedic Surgery, Tohoku University School of Medicine[1)], Tohoku Rosai Hospital[2)] and Honma Memorial Tohoku Orthopaedic Hospital[3)]
Department of Medical Engineering and Cardiology, Institute of Development, Aging and Cancer, Tohoku University[4)]
Sendai, Japan
Corresponding author: Hirotaka Sano, MD, E-mail: staka@mail.tains.tohoku.ac.jp

Abstract— To elucidate the pathogenetic roles of estrogen in the rupture of anterior cruciate ligament (ACL), the hormonal effects of estrogen on the material properties of ACL tissue should be fully clarified.

In 40 ovariectomized Japanese white rabbits, serum estrogen level was controlled by the intramuscular injection of estradiol. They were divided into 4 groups according to the dose of administered estradiol (Groups L, M, H and C). Intramuscular injection of 17β-estradiol was performed 1, 2, 3 and 4 weeks after surgery with the doses in Groups L, M, and H were 50, 100, and 500 μg/kg. For Group C, which served as control, no estradiol was administered. After 5 weeks from the overiectomy, lateral portion of ACL was harvested and fixed with 10% neutralized formalin and embedded in paraffin. The specimens were cut perpendicularly to the ligament fibers in the thickness of 10 μm both for routine histologic staining and SAM measurement.

In the measurement of SAM, Group M indicated the lowest value of tissue sound speed among 4 groups, which could be interpreted as the lowest Young's modulus. A statistically significant difference was found in the tissue sound speed between Groups C and M ($p=0.028$). We assumed that estrogen might constitute one of the pathogenetic factors of the ACL ruptures in the female athletes.

Keywords- anterior cruciate ligament, rupture, female, sound speed, scanning acoustic microscope

I. Introduction

Previous epidemiologic studies revealed that the ruptures of anterior cruciate ligament (ACL) were more frequently seen in female athletes than in male athletes [10]. In 1997, Bjordal reported that the ACL rupture rate in female soccer players was almost twice as high as that in males [1]. Among high school basketball players, the incidence of ACL rupture was reported as more than three times higher in female athletes than in male athletes [8].

To explain this sex difference, a number of pathogenetic factors have been proposed including lower limb alignment, shape of the intercondylar notch, joint laxity, hormonal effects, ligament size and body weight, etc [2], [3], [5], [16], [19]. However, the principal pathogenetic factor for the sex difference still remains unclear.

Given these controversies, the authors developed an estrogen-controlled rabbit model to clarify the hormonal effects of estrogen on tissue material property of ACL [4]. In this model, all animals were ovariectomized and then divided into 4 groups according to the administrated dose of estradiol. In the current study, we measured the tissue sound speed of their ACL, which closely correlates to their Young's modulus, using a scanning acoustic microscope (SAM). The purpose of this study was to compare the tissue sound speed between these 4 animal groups.

II. Materials and Methods

Animal model

The experimental procedures were approved by the committee for animal experimentation, Tohoku University School of Medicine.

Forty age-matched female Japanese white rabbits (32 weeks old) were used for the current project. Their average body weight was 4.3 (SD 0.43) kg. All were ovariectomized under general anesthesia using an intramuscular injection of ketamine hydrochloride (0.5 mg/kg) and xylazine (1.0 mg/kg). Each rabbit was housed in a cage individually under the same conditions, including room temperature, humidity, food and water. To prevent postoperative infection, enrofloxacin (5 mg/kg) was injected once a day into the back muscle for 3 days postoperatively.

The animals were divided into 4 groups (10 in each group) according to the dose of administered estradiol (low, medium, high and control: L, M, H and C). One rabbit in Group M died due to an anesthetic problem during surgery, thus this animal was excluded from analysis. In the other 39 rabbits, no postoperative infections were seen. Intramuscular injection of 17β-estradiol (Ovahormon depot®, Teikoku Hormone Manufacturing Co., Ltd. Japan) was performed 1, 2, 3 and 4 weeks after surgery. The doses of 17β-estradiol in Groups L, M, and H were 50, 100, and 500 μg/kg. For Group C, which served as control, neither estradiol nor any types of vehicles were administered.

Preparation of the specimens

All rabbits were killed with an overdose of pentobarbital sodium 5 weeks after the ovariectomy. The right hind limb was disarticulated at the hip, and the knees were dissected to expose the ACL. The ACL was divided into the lateral (lACL) and the medial portions (mACL). The femur-mACL-tibia complex was used for the biomechanical testing in our previous study [4], whereas lACLs were used for the current study. The specimens of lACL were fixed in 10% neutralized formalin and embedded in paraffin. Then, they were cut perpendicularly to the ligament fibers in the thickness of 10μm. Serial sections were made both for the SAM measurements and routine histologic staining including haematoxylin-eosin and elastica-Masson.

Measurement of the tissue sound speed of the lACL

A SAM system specially developed in Tohoku University, operating in the frequency range of 50-150 MHz, was used for this study [11-15]. The sections for SAM measurements were mounted on glass slides but not covered by cover slips. The paraffin was removed from the sections by the graded alcohol method prior to the ultrasonic measurement. Distilled water was used as the coupling medium, which maintained the specimen at 20°C during the measurement procedure. A single ultrasound pulse of 5 ns width was emitted and received by the same transducer above the specimen. The reflections from the tissue surface and those from the interface between the tissue and glass were introduced into a digital oscilloscope. Four values of the time taken for a pulse response at the same point were averaged in the oscilloscope in order to reduce the noise in the measurement. The transducer was mounted on an X-Y stage with a microcomputer board that was driven by the computer installed in the digital oscilloscope. The X-scan was driven by a linear servo motor, and the Y-scan was driven by a stepping motor. The area of measurement was 2.4 × 2.4 mm (300 × 300 pixels).

It is known that tissue sound speed is directory proportional to the square root of its Young's modulus as following equation shows,

$$c = \sqrt{\frac{E(1-\sigma)}{\rho(1+\sigma)(1-2\sigma)}}$$

(c: sound speed, E: Young's modulus, ρ: density, σ: Poisson's ratio).

To measure the tissue sound speed, SAM system required to look up three reflection data directory from the glass surface. Thus, three reference points without lACL tissue were determined manually on the monitor. Then, a two-dimensional distribution of sound speed in a specimen was displayed and saved as an image file using a color-coded scale. A gray scale image was also saved as an image file for further quantification of the tissue sound speed.

Quantification of tissue sound speed of ACL

To exclude the artifacts caused during the cutting process, the area where ligament tissue was properly transected was determined histologically as the region of interest (ROI). In each specimen, a gray-scale image was imported to the commercial software, Adobe Photoshop (version 7.0). With this image, the average value of density (between 0 and 255) of ROI was measured 5 times using the analysis option, "histogram". Then, the mean value of these 5 measurements (*mean density*) in each specimen was converted again to the sound speed (*mean sound speed*). Then, the *mean sound speed* was compared between the 4 animal groups to find out whether estrogen altered tissue elasticity of lACL or not.

Statistical analyses

Statview 5.0 (SAS Institute Inc.) was used for the statistical analyses in the current study. The Dunnett T3 test was used to determine the differences in the tissue sound speed among 4 animal groups. Differences were considered as statistically significant when the p-value was less than 0.05.

III. Results

A two-dimensional distribution of the tissue sound speed was successfully measured with SAM (**Figure 1**). All 3 estrogen-administrated animal groups (Groups L, M and H) indicated lower sound speed than that of Controls (Group C). Especially, Group M indicated the lowest value of the tissue sound speed among 4 groups, which could be interpreted as the lowest Young's modulus. A statistically significant difference was found in the tissue sound speed between Groups C and M ($p=0.028$, **Table 1**).

IV. Discussion

The pathogenetic roles of estrogen in ACL ruptures have not been fully clarified yet. Controversies still continues whether estrogen alters the mechanical properties of the ACL tissue or not. In 1997, Liu et al. reported that the presence of estrogen receptors was evident in the nuclei of synoviocytes, fibroblasts and cells in the blood vessel walls in ACL. They concluded that estrogen had some effects on both the cell composition and the histological structure [7]. Slauterbeck et al. investigated the relationship between the administrated dose of estrogen and the mechanical properties of the ACL using the ovariectomized rabbit model. They concluded that estrogen might alter the biomechanical strength of ACL [17]. More recently, Wojtys et al. reported that the incidence of ACL ruptures in the female athletes was closely correlated to the menstrual cycle [20]. All these findings supported the hypothesis that estrogen plays an important role in the ACL ruptures of female athletes. On the other hand, both Strickland et al. [18] and Rau et al. [9] reported that estrogen might not alter the material properties of ACL, especially within normal physiological range.

Based on these controversies, the authors tested biomechanical strength of femur-mACL-tibia complex in the estrogen-controlled rabbit models in our previous study. However, no significant differences in the ultimate tensile stress were found between any estradiol-administered group and Group C [4]. In the conventional biomechanical testing procedure, the femur-mACL-tibia complex was tested as one unit. Failure was occurred at the insertion in all specimens during the tensile testing. We assumed that the ultimate tensile stress measured in this study might not be directory reflected the alteration in the collagen fibers of ACL.

Since the estrogen receptors were localized in the ligament proper (i.e., nuclei of synoviocytes, fibroblasts and cells in the blood vessel walls) [6], the tissue elasticity of ligament proper should be measured at a microscopic level to clarify the direct effects of estrogen on ACL. Thus, in the current study, we focused on the ligament proper of lACLs and measured their elasticity using SAM. Our results clearly demonstrated that all 3 estradiol-administered groups showed lower sound speed than that of Group C. Moreover, a significant difference in the tissue sound speed was seen between Groups M and C. In other words, the ligament proper of Group M indicated the softest material property among 4 animal groups.

Based on these results, we assumed that estrogen might constitute one of the pathogenetic factors of the ACL ruptures in the female athletes. Further studies with lager number of animals will be needed to clarify the dose-dependent relationship between estrogen and the material properties of ACL.

V. Acknowledgments

The authors thank Mr. Katsuyoshi Shoji, Ms. Michiko Fukuyama in the Department of Orthopaedic Surgery, Tohoku University School of Medicine for their technical assistance.

Figure 1-a, b, c: Typical two-dimensional distribution pattern of tissue sound speed in lACL (Sample No.40-2, Group H).

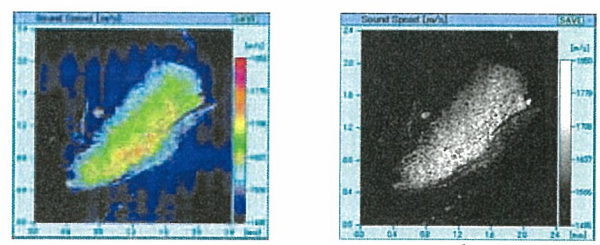

a b

c

a: SAM image with a color-coded scale, b: SAM image with a gray scale, c: haematoxylin-eosin staining (The circular area indicates the region of interest).

Table 1: Mean tissue sound speed and SD of lACLs in 4 animal groups

	Group C	Group L	Group M	Group H
Mean sound speed (m/s)	1727	1683	1665*	1690
SD	32	53	63	56

All three estrogen-administrated groups (Groups L, M and H) represented lower sound speed than that of Group C (Controls). A statistically significant difference was found between Group C and Group M (*p=0.028).

REFERENCES

[1] J.M. Bjordal, F. Arnly, B. Hannestad, T. Strand, Epidemiology of anterior cruciate ligament injuries in soccer. Am. J. Sports Med., **25** (1997) 341-345.

[2] T.G. Grace, E.R. Sweetser, M.A. Nelson, L.R. Ydens, B.J. Skipper, Isokinetic muscle imbalance and knee-joint injuries. A prospective blind study. J. Bone Joint Surg. (Am) **66** (1984) 734-740.

[3] M.R. Hutchinson, M.L. Ireland, Knee injuries in female athletes, Sports Med. **19** (1995) 288-302.

[4] T. Komatsuda, H. Sano, Does estrogen alter the mechanical properties of the anterior cruciate ligament ? Acta Orthop Scand, *in press*.

[5] A.S. Levy, M.J. Wetzler, M. Lewars, W. Laughlin, Knee injuries in women collegiate rugby players. Am. J. Sports Med., **25** (1997) 360-362.

[6] S.H. Liu, R.A. Al-Shaikh, V. Panossian, R.S. Yang, S.D. Nelson, N. Soleiman, G.A. Finerman, J.M. Lane, Primary immunolocalization of estrogen and progesterone target cells in the human anterior cruciate ligament. J. Orthop. Res., **14** (1996) 526-533.

[7] S.H. Liu, R.A. Al-Shaikh, V. Panossian, G.A. Finerman, J.M. Lane, Estrogen affects the cellular metabolism of the anterior cruciate ligament. A potential explanation for female athletic injury. Am. J. Sports Med., **25** (1997) 704-709.

[8] D.F. Messina, W.C. Farney, J.C. DeLee, The incidence of injury in Texas high school basketball. A prospective study among male and female athletes. Am. J. Sports Med., **27** (1999) 294-299.

[9] M.D. Rau, D. Renouf, D. Benfield, D.D. Otto, G.M. Thornton, V.J. Raso, K.M. Bagnall, Examination of the failure properties of the anterior cruciate ligament during the estrous cycle. Knee, **12** (2005) 37-40.

[10] H. Roos, M. Ornell, P. Gärdsell, L.S. Lohmander, A. Lindstrand, Soccer after anterior crusiate ligament injury – an incompatible combination? A national survey of incidence and risk factors and a 7-year follow-up of 310players. Acta Orthop. Scand., **66**, (1995) 107-112.

[11] Y. Saijo, H. Sasaki, H. Okawai, D. Nagamura, M. Tanaka, Acoustic Properties of the Normal and Pathologic Myocardium by Scanning Acoustic Microscopy. Jpn J. Med. Ultrasonics, **22** (1995) 29-40.

[12] Y. Saijo, H. Okawai, H. Sasaki, S. Masaaki, C.S. Jorgensen, S. Nitta, Application of Acoustic Microscopy for Assessing Stress Disrtribution in Atherosclerotic Plaque. Ann. Biomed. Eng., **29** (2001) 1048-1053.

[13] Y. Saijo, H. Sasaki, N. Hozumi, K. Kobayashi, M. Tanaka, T. Yambe, Sound speed scanning acoustic microscopy for biomedical applications. Technol. Health Care, **13** (2005) 261-267.

[14] Y. Saijo, C.S. Jorgensen, E. Falk, Ultrasonic tissue characterization of collagen in lipid-rich plaques in apoE-deficient mice. Atherosclerosis, **158** (2001) 289-295.

[15] Y. Saijo, M. Tanaka, H. Okawai, H. Sasaki, S.I. Nitta, F. Dunn, Ultrasonic tissue characterization of infarcted myocardium by scanning acoustic microscopy. Ultrasound Med. Biol., **23** (1997) 77-85.

[16] P. Schantz, E. Randall-Fox, W. Hutchison, A. Tyden, P.O. Astrand, Muscle fibre type distribution, muscle cross-sectional area and maximal voluntary strength in humans. Acta Physiol. Scand., **117** (1983) 219-226.

[17] J. Slauterbeck, C. Clevenger, W. Lundberg, D.M. Burchfield, Estrogen level alters the failure load of the rabbit anterior cruciate ligament. J. Orthop. Res., **17** (1999) 405-408.

[18] S.M. Strickland, T.W. Belknap, S.A. Turner, T.M. Wright, J.A. Hannafin, Lack of hormonal influences on mechanical properties of sheep knee ligaments. Am. J. Sports Med., **31** (2003) 210-215.

[19] E.M. Wojtys, L.J. Huston, T.N. Lindenfeld, T.E. Hewett, M.L. Greenfield, Association between the menstrual cycle and anterior cruciate ligament injuries in female athletes. Am. J. Sports Med., **26** (1998) 614-619.

[20] E.M. Wojtys, L.J. Huston, M.D. Boynton, K.P. Spindler, T.N. Lindenfeld, The effect of the menstrual cycle on anterior cruciate ligament injuries in women as determined by hormone levels. Am. J. Sports Med., **30** (2002) 182-188.

Image Processing for Scanning Type Biological Ultrasonic Microscope Considering Its Beam Characteristics

K. Kobayashi T.Ishiguro
Honda Electronics Co., Ltd.
Toyohashi, Japan

Y. Saijo
Tohoku Univ.
Sendai, Japan

N.Hozumi
Aichi Inst. of Technology
Toyota, Japan

Abstract– **We have been developing a biological ultrasonic microscope with a high lateral resolution.**
An acoustic pulse is transmitted by a scanning transducer to a substrate on which a thin slice of a tissue is embedded. The transducer has a minute curvature in order to focus an acoustic beam with a high frequency component. It may be fabricated by MEMS technology; however from the point of view of engineering, it may not be easy to guarantee the reproducibility of beam pattern as specified. In a high frequency range, a small error in fabrication will lead to a big difference in beam pattern which strongly affects the observed image. Using newly proposed methodology to observe a well-defined pin-hole, we found that each commercial single probe transducer with the same specification has a unique beam pattern. In addition, the pattern was not always concentric. Consequently, we proposed a method to compensate the image that was obtained using an eccentric beam pattern. A clearer image was successfully obtained after the compensation.A clearer image was successfully obtained after the compensation.
Keywords: biological tissue; beam form; micro-scale imaging.

I. INTRODUCTION

Pulse excitation ultrasonic sound-speed microscopes are useful as the quantitative evaluation equipment for tissue sound-speed. They use pulse waves for measurement of tissue sound-speed, and therefore use polymer transducers to achieve highly sensitive measurements with the pulse waves. To make a focused transducer using polymer piezoelectric film, the film is adhered to a metal bar that is processed to be concave according to the focal length. Sometimes the ideal focus cannot be made due to thickness of adhesive and film creases. It is impossible to generate polymer transducers for 100 MHz or higher frequencies, and the current pulse excitation ultrasonic sound-speed microscopes use transducers of 80 MHz and have a resolution of 18 μm. In pathology departments where tissue observations are implemented, optical microscopes are generally used. It is difficult to determine tissue structures in ultrasonic images with a resolution of 18 μm, because the resolution differs from that of commonly used optical microscopes. To solve this, we measured directional properties of the ultrasonic transducer and used them for improvement of blurred images. The improvement method is reported below.

II. PRINCIPLE

When an image is created by sending and receiving ultrasonic waves with an ultrasonic microscope, the resultant image is more unclear than the actual structure, as shown in Figure-1, due to directional properties of the ultrasonic transducer. The unclear image is an image obtained by applying the directional property function of the transducer to the true structure as a transfer function.

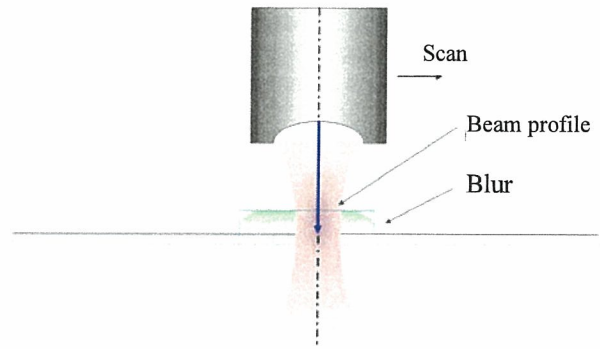

Figure-1 Blur under an ultrasonic microscope

When this blur is captured one-dimensionally, it is expressed as shown in Figure-2; where the true value is convolved by the transfer characteristic H.

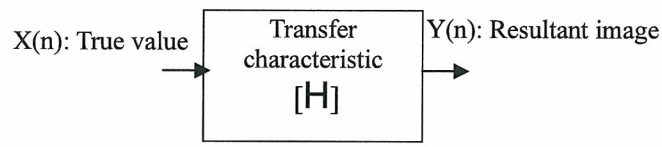

$$y(n) = \sum h(i)x(n-i)$$

Figure-2 Mechanism of blur

When this is considered two-dimensionally, the relationship between the true acoustic intensity image and the actually observed acoustic intensity image is expressed as:

$$\text{actual}(x, y) = \iint h(u, v)\,\text{ideal}(x-u, y-v)\,du\,dv$$
$$= h(x,y) * \text{ideal}(x,y) \quad (1)$$

ideal(x, y) : True acoustic intensity image
actual(x, y) : Actually observed acoustic intensity image
h(x, y) : Transfer function of the observation system
(* indicates convolution.)

When a focus is made at a point on the view plane in sending and receiving ultrasonic waves, the transfer function becomes a delta function,

$$h(x, y) = \delta(x, y) = 1 \{x = 0, y = 0\}$$
$$0 \{ \text{ else } \}$$

$$actual(x, y) = ideal(x, y)$$

and the observed acoustic intensity image accords with the true acoustic intensity image. On the other hand, when a focus is not made at a point but spreads on the view plane, the transfer function has the frequency dependency and has a characteristic that signals are more attenuated as the frequency becomes higher. As a result, the observed image becomes blurred and becomes different from the true image. Though the signal components are attenuated at higher frequencies, they will not be lost completely.

By applying the Fourier transform to equation (1), derive the relationship in the frequency domain as follows:

$$ACTUAL(\omega x, \omega y)=(\omega x, \omega y) \bullet IDEAL(\omega x, \omega y) \quad (2)$$

$$IDEAL(\omega x, \omega y) = FT\{ideal(x, y)\}$$
$$ACTUAL(\omega x, \omega y) = FT\{actual(x, y)\}$$
$$H(\omega x, \omega y) = FT\{h(x, y)\}$$

(FT{} indicates the Fourier transform in {}.)

This transforms the convolution relationship in equation (1) to a simple product relationship in equation (2). This way, restoration of the true image from an observed image in the frequency domain is expressed by the following formula, and an image in the actual image domain can be obtained through the inverse Fourier transform of the result.

$$IDEAL(\omega x, \omega y)= \{1/H(\omega x, \omega y)\} \bullet ACTUAL(\omega x, \omega y) \quad (3)$$

$$ideal(x, y) = IFT\{IDEAL(\omega x, \omega y)\}$$

(IFT{} indicates the inverse Fourier transform in {}.)

Restoration requires the reverse characteristic of the transfer characteristic. Using a sample from which the true image can be assumed, determine the reverse characteristic from the assumed image and the actually observed image in advance.

$$\{1/H(\omega x, \omega y)\} = IDEAL\_ref(\omega x, \omega y)/ACTUAL\_ref(\omega x, \omega y) \quad (4)$$

$$IDEAL\_ref(\omega x, \omega y) = FT\{ideal\_ref(x, y)\}$$
$$ACTUAL\_ref(\omega x, \omega y) = FT\{actual\_ref(x, y)\}$$

To be exact, it is necessary to determine equation (4) in consideration of not only the amplitude information but also the phase information (as a complex number). But the blur characteristic is almost symmetric about a point, so determine equation (4) simply as an amplitude spectrum ratio, disregarding the phase information.

$$\{1/H(\omega x, \omega y)\} = Amp\{IDEAL\_ref(\omega x, \omega y)\}/Amp\{ACTUAL\_ref(\omega x, \omega y)\} \quad (5)$$

(Amp indicates the amplitude component in {}.)

The reverse characteristic is obtained as a scalar value, and can be handled as a simple restoration gain table in equation (3).

III. SAMPLE USED FOR REFERENCE

As a reference for determining the restoration gain table, we used a metal sample through which a pinhole of a diameter of 200 μm passes as shown in Figure-3 (a). From the data measured under an optical microscope, we assumed the true image on the assumption that the acoustic intensity in the pinhole is zero (0) and the acoustic intensity in parts other than the pinhole is uniform and equal to the average acoustic intensity in a part sufficiently away from the pinhole in the actually observed image. Figure-4 (b) shows an image actually observed under an ultrasonic microscope.

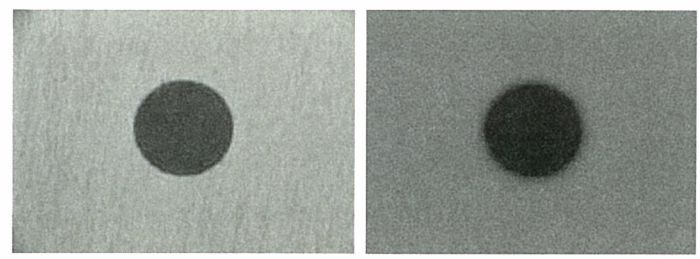

(a) Optical image (b) Ultrasonic image

Figure-3 Optical image and ultrasonic image of the reference of hole

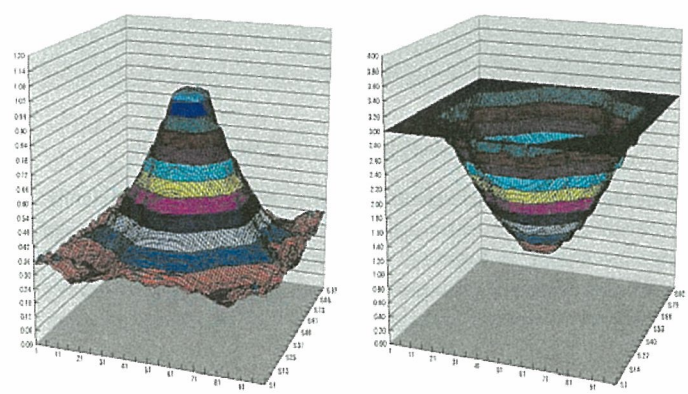

(a) Frequency characteristic of blur (b) Frequency characteristic of restoration

Figure -4 Frequency characteristic of blur and frequency characteristic of restoration

IV. LIMITATION OF RESTORATION GAIN TABLE

The transfer function of blur has a characteristic that signal components are more attenuated at higher frequencies as shown in Figure-4 (a). On the other hand, the restoration gain table becomes larger at higher frequencies. However, it is impossible to completely prevent entry of noise in actual acoustic intensity measurements, and it is necessary to limit the restoration gain table value. Otherwise, the effort to restore attenuated signals has the opposite effect of emphasizing noise components and deteriorating the image quality.

The evaluation on the observed image of the pinhole sample used for reference indicates that the noise components are equal to or higher than the signal components in the bands where the signal components are reduced to 1/5 or lower due to blur. Based on this result, we also assumed entry of more noises, and limited the restoration gain table value to three times as shown in Figure-4 (b).

V. RESULT

Figure-5 shows the result of restoring the ultrasonic observation image of a hole used for reference by utilizing the measured blur function. Figure-6 shows the restored image of a material with a circle of about 130 μm diameter around the same 100 μm hole. The hole and surrounding circle could be resolved with a resolution of 18 μm and observed at 100 MHz.

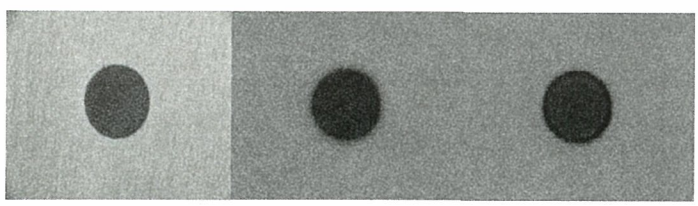

Figure-5 Improvement of the reference image

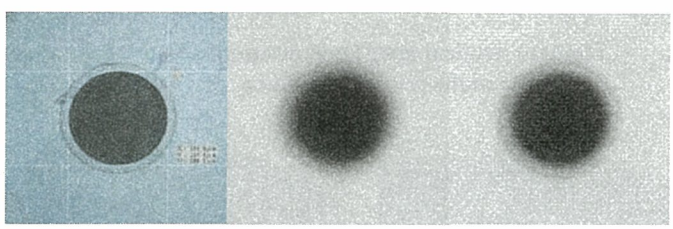

Figure-6 Improved image of a hole with link

When we treated observation examples of actual body tissues, we could eliminate blurs and obtain images close to optical images as shown in Figure-7 (esophagus), Figure-8 (mammary gland) and Figure-9 (stomach). These images were evaluated to be closer to optical images and easier to be judged in clinical use.

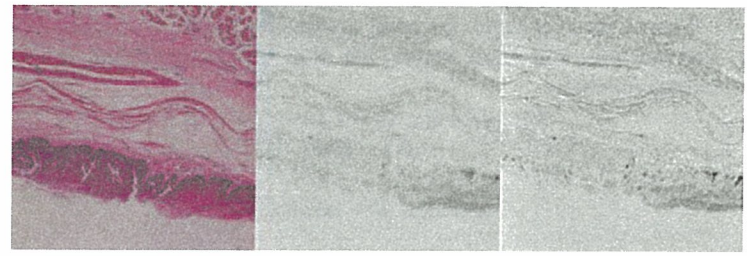

Figure-7 Improved image of body tissue (esophagus)

Figure-8 Improved image of body tissue

Figure-9 Improved image of body tissue (stomach)

VI. SUMMARY

Sharpening of images in consideration of the directional properties of transducer has been enabled by a simple arithmetic process by using the 2DFFT technique. It was found that high-resolution observation can be achieved without side-effects in actual observation by considering the SN when a reference image is captured and preventing noise from being included in determination of correction value. We will apply this method to high-frequency transducers for application in cell observation and other fields that require high resolution.

Non-mineralized fibrocartilage shows the lowest elastic modulus in the rabbit supraspinatus tendon insertion: Measurement with scanning acoustic microscopy

Hirotaka Sano, MD,[a] Yoshifumi Saijo, MD,[b] and Shoichi Kokubun, MD,[a] *Sendai, Japan*

The acoustic properties of rabbit supraspinatus tendon insertions were measured by scanning acoustic microscopy. After cutting parallel to the supraspinatus tendon fibers, specimens were fixed with 10% neutralized formalin, embedded in paraffin, and sectioned. Both the sound speed and the attenuation constant were measured at the insertion site. The 2-dimensional distribution of the sound speed and that of the attenuation constant were displayed with color-coded scales. The acoustic properties reflected both the histologic architecture and the collagen type. In the tendon proper and the non-mineralized fibrocartilage, the sound speed and attenuation constant gradually decreased as the predominant collagen type changed from I to II. In the mineralized fibrocartilage, they increased markedly with the mineralization of the fibrocartilaginous tissue. These results indicate that the non-mineralized fibrocartilage shows the lowest elastic modulus among 4 zones at the insertion site, which could be interpreted as an adaptation to various types of biomechanical stress. (J Shoulder Elbow Surg 2006;15:743-749.)

Previous clinical studies revealed that most of the rotator cuff tears were seen close to the insertion site of the supraspinatus tendon.[4,26] To elucidate the pathogenesis of the tendon tearing, both the histologic and the biomechanical characteristics of the insertion site should be fully clarified. Histologically, the supraspinatus tendon insertion consists of 4 zones, including the tendon proper, non-mineralized fibrocartilage, mineralized fibrocartilage, and bone.[5] This 4-zone structure constitutes a histologic transition from soft tissue (tendon) to bone. It is believed that the histologic transition at this site is accompanied by a change in the tissue material properties.[3,12] However, the actual material properties of the tendon insertion have not been measured yet because of its complicated histologic architecture. Recently, we developed finite element models of the supraspinatus tendon with its insertion.[22,27] Because no data was available for the material properties of fibrocartilage, medium values between the tendon and the cancellous bone were calculated and used for the analysis. The actual data of the material properties of fibrocartilage would improve the quality of these types of stress analyses.

Scanning acoustic microscopy (SAM) was first developed by Lemons and Quate in 1973[11] to visualize opaque materials at the microscopic level. Since then, we have been developing SAM for medicine and biology to measure tissue acoustic properties. It is known that tissue acoustic properties closely correlate to mechanical properties. Tissues representing heterogeneous histologic architecture could especially be assessed using SAM. In cardiology, SAM has already been applied for various types of soft tissues, that is, cardiac muscles, arterial plaques, vascular walls, etc.[16,17] On the other hand, the application of this technology in the orthopedic field has been limited to undecalcified bony specimens.[6,25] Recently, SAM was first applied to measure the acoustic properties of the supraspinatus tendon.[21] However, because this study only dealt with the tendon and not the 4-zone structure at its insertion, the transition of the tissue material properties still remains unclear.

Therefore, we attempted to describe the transition of the acoustic properties in the whole 4-zone structure at the insertion site of the rabbit supraspinatus tendon. We further attempted to determine the biomechanical characteristics of the supraspinatus tendon insertion.

MATERIALS AND METHODS

Preparation of the specimens

The supraspinatus tendon insertions of 3 Japanese white rabbits were used for the SAM measurement. They were all

From the [a]Department of the Orthopaedic Surgery, Tohoku University School of Medicine and [b]Department of Medical Engineering and Cardiology, Institute of Development, Aging and Cancer, Tohoku University.

Reprint requests to: Hirotaka Sano, MD, Department of Orthopaedic Surgery, Tohoku University, School of Medicine, 1-1 Seiryo-machi, Aoba-ku, Sendai, 980-8574, Japan (E-mail: *staka@mail.tains.tohoku.ac.jp*).

1058-2746/2006/$32.00
doi:10.1016/j.jse.2005.12.008

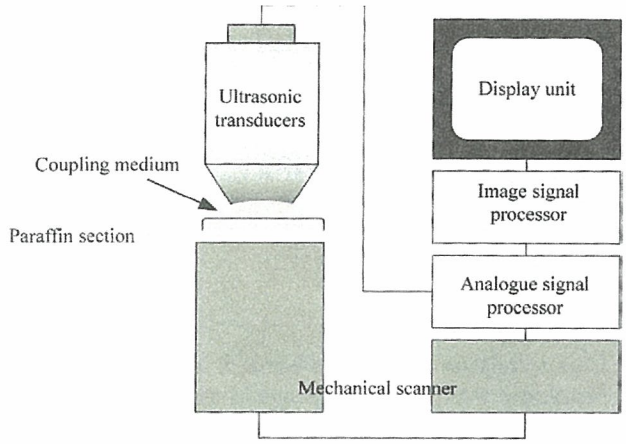

Figure 1 Block diagram of the system of the scanning acoustic microscopy.

6-month-old males, and their body weight was 3.2-3.5 kilograms. After euthanasia with an overdose of pentobarbital, bilateral supraspinatus tendons attached to the humeral heads were removed.

The specimens were cut parallel to the supraspinatus tendon fibers with a microcutting machine (EXAKT, Germany). The anterior parts of the supraspinatus tendons were fixed with 10% neutralized formalin for 12 hours. Because decalcification might alter the acoustic properties of the soft tissues, the humeral head was removed except for the insertion site to avoid decalcification. After embedding in paraffin, the specimens were cut at a thickness of 5 μm along the supraspinatus tendon fibers. Serial sections were made to compare the tissue acoustic properties to the histologic and the immunohistochemical characteristics.

Histologic investigations

Hematoxylin-eosin (HE) staining was routinely employed to assess the overall histologic structure. Immunohistochemical staining was also performed to confirm the presence of types I and II collagen at the insertion site. The avidin-biotinylated peroxidase complex method was employed using the monoclonal antibodies against types I and II collagens (anti-hCL(I) and anti-hCL(II), purified IgG, FUJI Chemical Industries Ltd., Toyama, Japan). Photographs were taken under the microscopy, and these were trimmed to create histologic images with areas identical to those of the SAM measurements.

SAM measurements

A specially developed SAM system, operating in the frequency range of 100-200 MHz, was employed for this study.[14,15] This system consists of 5 parts, viz. (1) ultrasonic transducers, (2) a mechanical scanner, (3) an analogue signal processor, (4) an image signal processor, and (5) a display unit (Figure 1). The focusing element is mechanically scanned at 60 Hz in a lateral direction (x) above the specimen, while the sample holder is scanned in the other lateral direction (y) for 8 seconds, thus providing 2-dimensional scanning. Images of the amplitude and phase are obtained in a 2-mm field of view. In the current study, we decided to focus on the articular surface of the supraspinatus tendon, because the entire width of the tendon could not be included in the single SAM measurement. Moreover, it has been known that the fibrocartilage is the most evident in the deep part of the tendon insertion but almost absent superficially.[3]

Distilled water was used as the coupling medium, which maintained the specimen at 20°C during the measurement procedure. The sections for SAM measurements were mounted on glass slides but not covered by coverslips. The paraffin was removed from the sections by the graded alcohol method prior to the ultrasonic measurement. Then, serial measurements were done with the SAM along the articular surface of the tendon from the insertion site to the musculotendinous junction. The data of the sound speed and the attenuation constant obtained were converted into color signals on the computer. Two-dimensional distribution patterns of those parameters were displayed and saved as an image file using color-coded scales. Then, these serial image files were connected together to reconstruct a single image from the insertion site to the musculotendinous junction.

The sound speed measured by SAM is defined by the following equation:

$$c = \sqrt{K/\rho} \qquad (1)$$

where c is the sound speed, K the elastic bulk modulus, and ρ the density. The relationship between the acoustics and a solid material can be described by modifying the above equation:

$$c = \sqrt{\frac{E(1-\sigma)}{\rho(1+\sigma)(1-2\sigma)}} \qquad (2)$$

where E is the Young's modulus and σ the Poisson's ratio. Equation 2 shows that the tissue sound speed, measured using SAM, is directly proportional to the square value of its Young's modulus.

RESULTS

Routine staining

The histologic specimens successfully included the area from the musculotendinous junction to the subchondral bone with the entire 4 zones of the insertion (Figure 2, a). In the tendon proper, the direction of the tendon fibers was longitudinal and nuclei were spindle shaped (fibroblasts). Although there was no distinct histologic border between the tendon proper and the non-mineralized fibrocartilage, the shapes of nuclei gradually changed to oval or round toward the non-mineralized fibrocartilage (chondrocytes). Between the non-mineralized and the mineralized fibrocartilage, there was a distinct blue line, the tidemark, seen histologically as a calcifying front (Figure 3, a).

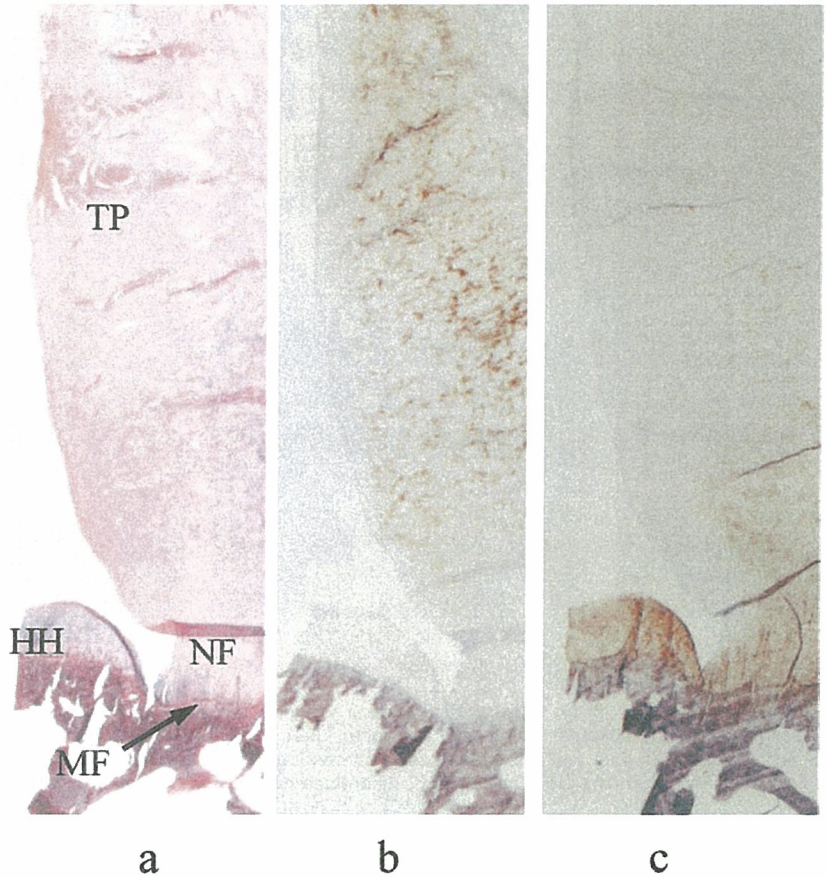

Figure 2 Histologic and immunohistochemical findings of the supraspinatus tendon and its insertion (Original magnification = ×1.25). (**a**) Hematoxylin-eosin; (**b**) type I collagen; (**c**) type II collagen. Type I collagen is positively stained in the tendon proper, whereas Type II collagen is localized in the fibrocartilage and the articular cartilage of humeral head. TP = tendon proper, NF = non-mineralized fibrocartilage, MF = mineralized fibrocartilage, HH = humeral head.

Collagen staining

Immunohistochemically, positive type I collagen was seen in the tendon proper. Between the tendon proper and the non-mineralized fibrocartilage, the predominant collagen type shifted from I to II (Figure 2, b, c). Type I collagen was not seen in the fibrocartilage (Figure 3, b). Additionally, both the non-mineralized fibrocartilage and the mineralized fibrocartilage were stained positively for type II collagen (Figure 3, c).

SAM measurements

The distribution of the sound speed and that of the attenuation constant showed almost identical patterns, which varied from zone to zone at the insertion (Figure 4, a, b). These 2 parameters reflected both the histologic architectures and the collagen types. In the tendon proper and the non-mineralized fibrocartilage, both the sound speed and the attenuation constant gradually decreased with the change in the predominant collagen type from I to II. The acoustic properties changed rapidly at the tidemark. In the mineralized fibrocartilage, they increased rapidly again with the mineralization of the fibrocartilaginous tissue (Figure 5, a, b). On the other hand, there were no differences in the acoustic properties between the mineralized fibrocartilage and the bone (Figure 5, a, b). The attenuation constant in both the mineralized fibrocartilage and the bone might have been beyond the upper limit of the SAM measurement. Table I summarizes the acoustic properties assessed in each zone.

DISCUSSION

There have been only a few reports published concerning the material properties of the supraspinatus tendon insertion.[7,13,20] In these studies, the entire bone-tendon complex was measured as one unit by conventional tensile testing procedures. More recently, Lee et al[10] measured the compressive stiffness of the human